Low Hesperian P_{CO2} constrained from in situ mineralogical analysis at Gale Crater, Mars

Thomas F. Bristow[a,1], Robert M. Haberle[b], David F. Blake[a], David J. Des Marais[a], Jennifer L. Eigenbrode[c], Alberto G. Fairén[d], John P. Grotzinger[e], Kathryn M. Stack[f], Michael A. Mischna[f], Elizabeth B. Rampe[g], Kirsten L. Siebach[e], Brad Sutter[h], David T. Vaniman[i], and Ashwin R. Vasavada[f]

[a]Exobiology Branch, NASA Ames Research Center, Moffett Field, CA 94035; [b]Planetary Systems Branch, NASA Ames Research Center, Moffett Field, CA 94035; [c]Solar System Exploration Division, NASA Goddard Space Flight Center, Greenbelt, MD 20771; [d]Department of Planetology and Habitability, Centro de Astrobiología, Madrid 28850, Spain; [e]Division of Geological and Planetary Sciences, California Institute of Technology, Pasadena, CA 91125; [f]Jet Propulsion Laboratory, California Institute of Technology, Pasadena, CA 91109; [g]Astromaterials Research and Exploration Science Division, NASA Johnson Space Center, Houston, TX 77058; [h]Jacobs Technology, Inc., NASA Johnson Space Center, Houston, TX 77058; and [i]Planetary Science Institute, Tucson, AZ 85719

Edited by Mark H. Thiemens, University of California, San Diego, La Jolla, CA, and approved December 27, 2016 (received for review October 6, 2016)

Carbon dioxide is an essential atmospheric component in martian climate models that attempt to reconcile a faint young sun with planetwide evidence of liquid water in the Noachian and Early Hesperian. In this study, we use mineral and contextual sedimentary environmental data measured by the Mars Science Laboratory (MSL) Rover *Curiosity* to estimate the atmospheric partial pressure of CO_2 (P_{CO2}) coinciding with a long-lived lake system in Gale Crater at ∼3.5 Ga. A reaction–transport model that simulates mineralogy observed within the Sheepbed member at Yellowknife Bay (YKB), by coupling mineral equilibria with carbonate precipitation kinetics and rates of sedimentation, indicates atmospheric P_{CO2} levels in the 10s mbar range. At such low P_{CO2} levels, existing climate models are unable to warm Hesperian Mars anywhere near the freezing point of water, and other gases are required to raise atmospheric pressure to prevent lake waters from being lost to the atmosphere. Thus, either lacustrine features of Gale formed in a cold environment by a mechanism yet to be determined, or the climate models still lack an essential component that would serve to elevate surface temperatures, at least locally, on Hesperian Mars. Our results also impose restrictions on the potential role of atmospheric CO_2 in inferred warmer conditions and valley network formation of the late Noachian.

Hesperian Mars | martian atmosphere | Mars Science Laboratory | Gale Crater | carbon dioxide

More than four decades of orbital imaging of Mars provide geomorphological evidence of a more active hydrological cycle and larger inventory of water during the Noachian and Early Hesperian (1, 2). The widespread distribution of hydrous clay minerals in martian terrains of this age and their subsequent demise provide pivotal supporting evidence (3, 4), but the clay mineral-bearing deposits also present a paradox in that carbonate minerals, expected coprecipitates in surficial settings in communication with a CO_2-bearing atmosphere, are typically absent (5). Atmospheric reconstructions using carbon isotopic measurements and global inventories of martian carbon also indicate 100s mbar CO_2 levels (5, 6). This leads to the question of how the surface of ancient Mars, faintly heated by a young sun, was kept warm enough to allow an active hydrological cycle, without substantial amounts of a key greenhouse gas in the atmosphere. However, the breadth of available constraints on carbon sinks (6) and potential clay mineral formation in subsurface settings uninfluenced by the atmosphere (7) introduce uncertainties to estimates and the periods to which they apply. In this work we use mineralogical and sedimentological data from ∼3.5 Ga martian lake sediments to obtain a reference point for the evolution of martian P_{CO2}.

During its traverse to the lower slopes of Aeolis Mons (informally known as Mt. Sharp), the MSL team documented a ∼70 m sedimentary section of mudstones, siltstones, sandstones, and conglomerates deposited by lakes and rivers on the floor of Gale crater between 3.8 and 3.1 Ga (8). Sedimentary rocks analyzed by the CheMin X-ray diffraction (XRD) instrument during the traverse share many of the same components including (*i*) crystalline silicates including pigeonite, intermediate calcic plagioclase, and olivine from a basaltic source or sources; (*ii*) poorly crystalline clay minerals; (*iii*) various Fe oxides including magnetite; (*iv*) Ca–sulfate minerals, which mainly occur in cross-cutting fractures and veins; and (*v*) an X-ray amorphous component (9, 10). Thus far, carbonate minerals have not been definitively detected in Gale Crater sedimentary rocks. This is surprising given the reactivity of minerals making up sediments to carbonic acid.

Of the phases present, smectitic clay minerals and magnetite provide a potential means of estimating ancient P_{CO2} by constraining dissolved inorganic carbon (DIC) levels in the pore fluids of Gale Crater sediments. It is proposed that isochemical alteration during the deposition of lacustrine mudstone at YKB involved dissolution of Fe^{2+}-bearing olivine (Fo_{62}) providing a source of Fe^{2+} and Mg^{2+} in pore waters for subsequent coeval precipitation of magnetite and Fe^{2+}-bearing, ferrian saponite–type clay minerals (9, 11–14). The detection of these secondary phases indicates anoxic to poorly oxidizing conditions (13), and places lower limits on the pore water activity of Fe^{2+} and Mg^{2+} released from olivine. Therefore, the thermodynamic stability fields of ferrian saponite and magnetite with respect to Fe and Mg carbonates can be used as the basis of estimates of atmospheric P_{CO2} at the time of Sheepbed deposition. Ferrian saponite and magnetite are thermodynamically unstable with respect

Significance

Approximately 3.5-Ga sedimentary rocks surveyed by the Mars Science Laboratory rover in Gale Crater, Mars, contain secondary mineral phases indicating aqueous alteration and release of cations from mafic minerals during sediment deposition in lakes. However, carbonate phases are not detected, and our model calculations indicate atmospheric CO_2 levels at the time of sediment deposition 10s to 100s of times lower than those required by climate models to warm early Mars enough to maintain surficial water. Our results offer a ground-based reference point for the evolution of martian atmospheric CO_2 and imply that other mechanisms of warming Hesperian Mars, or processes that allowed for confined hydrological activity under cold conditions, must be sought.

Author contributions: T.F.B., D.F.B., J.P.G., D.T.V., and A.R.V. designed research; T.F.B. performed research; T.F.B., R.M.H., D.F.B., D.J.D.M., J.L.E., A.G.F., J.P.G., K.M.S., M.A.M., E.B.R., K.L.S., B.S., D.T.V., and A.R.V. analyzed data; and T.F.B. wrote the paper.

The authors declare no conflict of interest.

This article is a PNAS Direct Submission.

Freely available online through the PNAS open access option.

[1]To whom correspondence should be addressed. Email: thomas.f.bristow@nasa.gov.

This article contains supporting information online at www.pnas.org/lookup/suppl/doi:10.1073/pnas.1616649114/-/DCSupplemental.

to Fe and Mg carbonates, such as siderite and magnesite, between 10^{-5} to 10^{-2} bar P_{CO2} depending on assumed activity of silica and Al^{3+} of pore waters (Fig. 1).

Estimates of P_{CO2} on the Archean (>2.5 Ga) Earth, derived from paleosols and banded iron formations, also use the thermodynamic stability of clay minerals and magnetite (17–19), but are criticized because they rely on assumptions of mineral equilibrium and do not account for enhanced delivery of carbon and reducing power to sediments via biological activity (20, 21). Metamorphic overprinting of original mineral assemblages in terrestrial rocks this old is ubiquitous and complicates interpretations further (22).

In many ways, deriving P_{CO2} estimates from Gale Crater sedimentary rocks is more straightforward than doing so in their terrestrial equivalents. Examination of ancient sediments at YKB shows that they, despite their age, have been subject to minimal burial diagenetic alteration and heated to no more than 70 °C (9, 12, 13) consistent with reconstructed burial history and estimates of ancient geothermal gradients (23). The observed persistence of smectite clay minerals, magnetite, levels of hematite at CheMin's detection limit of ∼1 wt % and absence of cation leaching in YKB sediments revealed by bulk geochemistry (9, 11) is inconsistent with pervasive postdepositional chemical weathering or alteration that may have otherwise had the potential to dissolve authigenic carbonate minerals.

In addition, MSL has not detected signs of biological influence on the Gale Crater sediments. In particular, the organic molecules observed by the Sample Analysis at Mars (SAM) instrument suite are extremely localized and restricted to simple structures (e.g., C1-C4 alkyl and single-ring aromatic hydrocarbons and chlorohydrocarbons; ref. 24) that lack source information. As such, they may be derived from meteoritic, abiogenic, or geologically reworked biological inputs to the sediments.

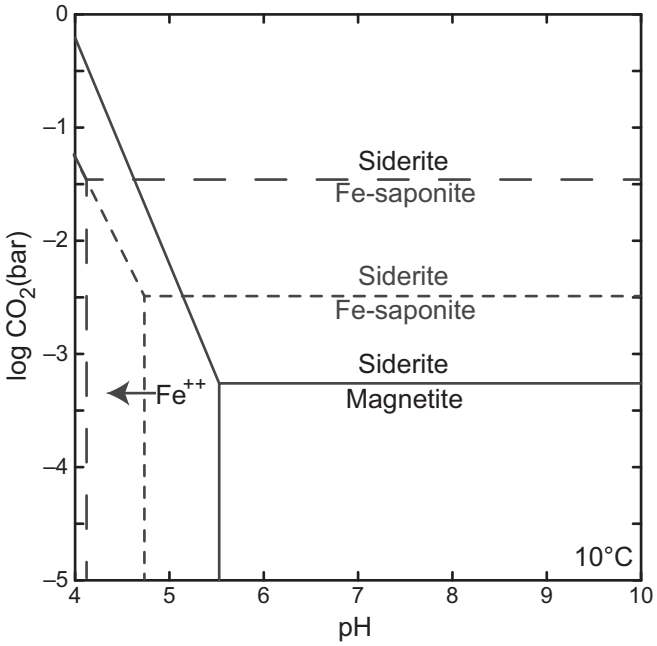

Fig. 1. Thermodynamic stability of secondary minerals (magnetite and Fe saponite) detected in the Sheepbed member, Yellowknife Bay with respect to siderite under varying pH and gaseous CO_2 levels. The threshold P_{CO2} at which siderite is favored over ferrian saponite is dependent on aqueous silica and Al^{3+} activity. The threshold is higher when $SiO_{2(aq)}$ is saturated with respect to amorphous silica (long dashed line) rather than quartz (short dashed line). In both cases Al^{3+} is set to saturation with respect to albite—reasonable given that the Sheepbed contains ∼20 wt % plagioclase feldspar (9). In drawing the stability boundaries for magnetite, redox state is set at the magnetite/hematite boundary, as detailed in the main text. All thermodynamic data come from the Lawrence Livermore National Laboratory dataset (15) with the exception of Fe saponite ($Na_{0.35}Fe_3Al_{0.35}Si_{3.65}O_{10}OH_2$) determined by Wilson et al. (16). Diagram produced using Geochemist Work Bench 9.

Assuming that sedimentary mineral assemblages were in thermodynamic equilibrium with the atmosphere remains problematic, however. Even with martian P_{CO2} levels above thermodynamic thresholds for carbonate stability, notoriously slow precipitation kinetics of Fe and Mg carbonates may have been a barrier to producing detectable quantities in Gale Crater sediments before burial and isolation from an atmospheric carbon source. For example, magnesite requires temperatures greater than ∼70 °C for direct precipitation in the laboratory (25). Siderite forms under ambient laboratory conditions at rates ∼4 orders of magnitude slower than calcite (26).

Here we take a step beyond assuming mineral equilibrium and combine estimated sedimentation rates, afforded by detailed sedimentary facies analysis (8, 12), with carbonate precipitation kinetics and observed mineralogy to estimate ancient P_{CO2} using a geochemical reaction–transport model.

Model Summary

Our models are constructed to determine threshold P_{CO2} levels that would permit the precipitation of detectable amounts of siderite by CheMin. For samples bearing the mixture of phases observed within Sheepbed mudstone (9), CheMin has a detection limit of ∼1 wt % siderite. The SAM instrument detects release of CO_2 upon sample heating, which can, in part, be derived from decomposition of carbonate minerals. The results of SAM analyses of YKB sediments provide no clear indication of Fe carbonate, but the expected CO_2 signal for carbonates may be masked by other CO_2 sources thus permitting the presence of Fe carbonates at abundances below the CheMin detection limit (27).

Precipitation rates and therefore accumulation of carbonates depend on the saturation state of pore water with respect to a particular carbonate phase (Ω), given by

$$\Omega_{carbonate} = \frac{[M^{2+}][CO_3^{2-}]}{[K_{sp}]}, \quad [1]$$

where K_{sp} is the solubility product of the carbonate in question and M^{2+} represents the concentration of the metal cation in pore water.

Ω is linked to carbonate precipitation rate ($R_{carbprec}$) by the expression,

$$R_{carbprec} = K_{carbprec}(\Omega_{carbonate} - 1)^n, \quad [2]$$

where $K_{carbprec}$ is the rate constant and n is the order of the reaction.

Our models calculate $[CO_3^{2-}]$ by simulating advection, diffusion, and reaction of DIC species, including precipitation of carbonate, in a one-dimensional porous sedimentary profile subject to active sedimentary accumulation and burial (detailed in *SI Text, Model Details*). Diffusion and advection from the upper model boundary actively replenish DIC (including CO_3^{2-}) lost from pore waters during carbonate precipitation and transport and, thus, are of critical importance in modeling the total carbonate accumulation. Upper model boundary conditions are set to simulate a well-mixed lake in equilibrium with an assigned P_{CO2} atmosphere. This is a valid representation given the absence of glaciogenic sedimentary features, such as dropstones, ice wedges, and glacial tills, in Gale lake deposits that would indicate ice cover, and the meter-scale thicknesses of delta deposits that indicate water depths of the same order (8).

We can make broad inferences about lake water chemistry at the time of YKB formation deposition. Salinity appears to have been low based on limited Cl and S concentration in the sedimentary

matrix and the lack of detection of evaporative minerals in the mudstone (9, 11, 12). This is compatible with bulk geochemical evidence of limited chemical alteration of sediments during erosion and transport from the source area (11). The observed stability of clay minerals and magnetite in the sediments implies circum-neutral pH pore waters (Fig. 1) that were not overwhelmed by hypothesized surficial sources of acidity sometimes invoked for Mars aqueous environments (28, 29). Thus, DIC speciation and concentrations at the upper model boundary (representing lake water) are calculated over a range of assigned pHs and atmospheric P_{CO2} levels, with the lowest pH of 5 corresponding to the lower stability field of magnetite (Fig. 1).

A variety of approaches to estimate the activity of metal cations required to calculate the saturation states and accumulation rates of carbonates are possible (Eqs. **1** and **2**). For example, in a full kinetic model, metal cation activities are calculated as a function of competing mineral dissolution and precipitation reactions, and in the case of Fe^{2+}, the redox state of pore waters. Although this approach provides the most mathematically complete model of a given system, the assigned kinetic parameters are subject to significant uncertainty. For instance, the rate laws governing saponite precipitation are unknown and must be guessed through comparison with other clay minerals that differ in terms of chemistry and crystal structure (e.g., ref. 30). Moreover, order-of-magnitude differences between kinetic rate laws determined in the laboratory and observed in natural systems are a well-documented challenge for reaction–transport models.

Alternatively, if the goal of the model is to obtain an absolute upper threshold of P_{CO2} consistent with nondetection of carbonates at Gale Crater, then our preferred hybrid kinetic model formulation becomes suitable. Calculating an upper P_{CO2} threshold requires a minimum bound on the activity of metal cations in solution. For the sediments at YKB, where evidence of magnetite and saponite precipitation at the time of deposition is documented, a minimum bound can be placed on Fe^{2+} activity in pore water by assuming that both magnetite and ferrian saponite are at or above saturation levels. Fig. S1 shows that with expected activities of silica and Al^{3+}, ferrian saponite is always supersatured when $[Fe^{2+}]$ is at saturation with respect to magnetite. Thus, $[Fe^{2+}]$ is calculated in the model assuming that pore waters are saturated with respect to magnetite. We note that in a full kinetic model $[Fe^{2+}]$ would approach magnetite saturation in a situation where precipitation of magnetite and saponite outcompeted siderite for $[Fe^{2+}]$.

To calculate pore water $[Fe^{2+}]$ based on magnetite saturation requires a redox constraint. Redox is assigned to the magnetite/hematite boundary, again minimizing $[Fe^{2+}]$ in the model profile, in keeping with the goal of obtaining an upper P_{CO2} threshold (Fig. S2). Formulating the model in this way is also consistent with detection of small amounts of hematite in YKB sediments (9). This state is represented by the following chemical reaction:

$$\text{Magnetite} + 2[H^+] = [Fe^{2+}] + [H_2O] + \text{Hematite}. \quad [3]$$

By calculating the equilibrium constant $K_{mag/hem}$ for reaction 3 at given temperature and salinity values and assuming H_2O activity of 1 a pH-dependent expression for $[Fe^{2+}]$ is obtained.

$$[Fe^{2+}] = K_{mag/hem} \cdot [H^+]^2. \quad [4]$$

$[Fe^{2+}]$ is calculated in the model profile at each time step based on pH using Eq. **4** allowing the saturation state with respect to siderite to be determined. Combining calculated $\Omega_{siderite}$ with the slowest kinetic rate law governing siderite precipitation available in the literature (Table S1), we determine the upper threshold of atmospheric P_{CO2} that would result in siderite being undetectable by CheMin in the YKB formation. Note that in configuring the model in this way it is assumed that siderite precipitation kinetics limit carbonate production; Fe^{2+} supplied by the dissolution of olivine does not. Fig. S3 shows this assumption is valid. Typical equilibrium outputs of a model run are shown in Fig. S4.

Results and Discussion

Fig. 2*A* shows upper P_{CO2} thresholds for siderite detection over a range of assigned water column pH and at various sediment accumulation rates. Water column pH has limited influence on rates of siderite production between values of 5 and 7 in our model. This is because siderite precipitation rate is determined by $\Omega_{siderite} = [Fe^{2+}][CO_3^{2-}]$, where at low pH small carbonate anion concentrations are compensated for by higher $[Fe^{2+}]$ required to maintain magnetite saturation (Fig. S2). Above pH 7, P_{CO2} thresholds decrease (Fig. 2*A*). To maintain high pH within a water column in equilibrium with the range of atmospheric P_{CO2} values investigated here requires elevated carbonate alkalinity and thus DIC. High DIC levels make diffusion and carbonate precipitation in the lower parts of modeled sedimentary

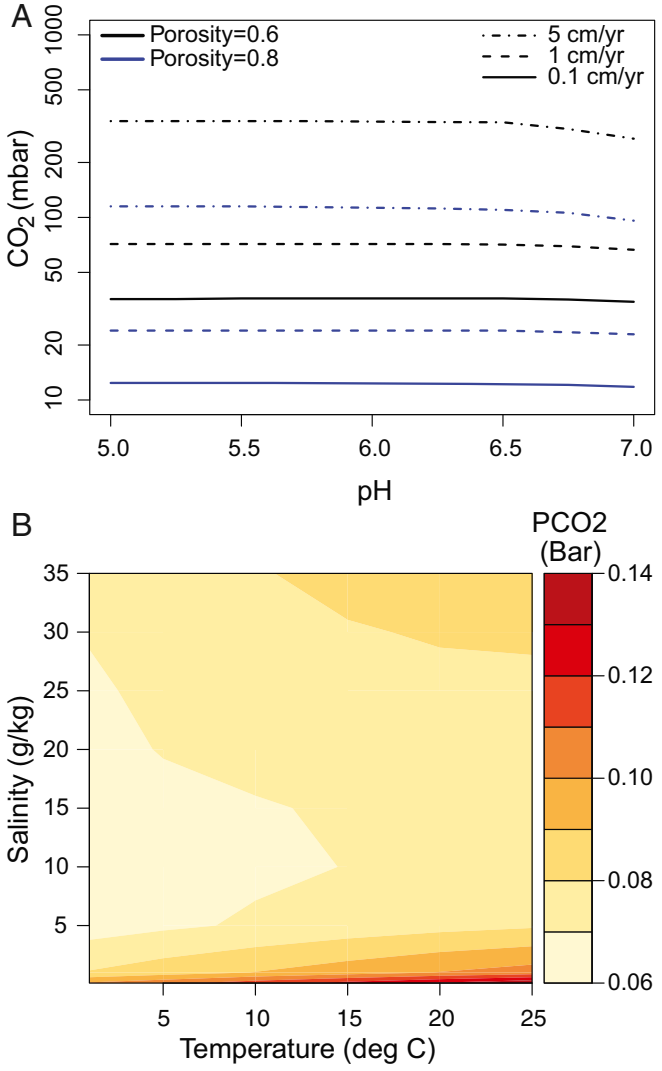

Fig. 2. (*A*) P_{CO2} required to produce 1 wt % siderite within model sedimentary profiles at various sediment accumulation rates, sediment porosities, and water column pH values. $[Fe^{2+}]$ is set to be saturated with respect to magnetite under redox conditions corresponding to the magnetite/hematite boundary. (*B*) Sensitivity of P_{CO2} thresholds to salinity and temperature with a burial rate of 1 cm/y and sedimentary porosity of 0.6.

profiles more efficient, lowering P_{CO2} thresholds. Because we aim to determine an upper constraint on P_{CO2} we focus our discussion on the P_{CO2} thresholds obtained assuming pH of lake waters between 5 and 7—the lowest values compatible with saponite and magnetite precipitation (Fig. 1).

Sedimentary porosity influences the rates of siderite production by controlling the quantity of pore water DIC available for reaction with Fe^{2+} released from olivine and rates of chemical diffusion within sediments, both of which generally increase with porosity. On Earth, mud deposits typically have initial porosities of between 60 and 80% (31). We have assigned a porosity value of 60% in our model profiles to obtain upper P_{CO2} thresholds (Fig. 2*A*). No significant sedimentary compaction is expected within ∼1.5–3 m model interval where carbonates form.

Calculated P_{CO2} thresholds are also highly sensitive to sediment accumulation rates, with faster rates permitting higher threshold atmospheric P_{CO2} levels (Fig. 2). We have no direct constraints on the rates of deposition of the YKB formation, but given the similarity of the sedimentary architecture with terrestrial fluvial–lacustrine deposits (8) we use compilations of thousands of lacustrine accumulation rates observed on Earth to obtain an upper limit for the YKB formation (31). Terrestrial lacustrine sedimentation rates span several orders of magnitude, with a dependence on the time span of accumulation (32). With accumulation times of 100s to 10,000 y estimated for the 1.5-m-thick Sheepbed member (12), accumulation rates as high as 5 cm/y are possible, with an average rate ∼0.1 cm/y (32). Lacustrine deposits with sedimentation rates >1cm/y make up <1% of available records. The highest rates are not sustainable for periods of more than ∼100 y, thus we use an upper sedimentation rate of 1 cm/y in calculating P_{CO2} estimates. We find that temperature and pore water salinity have a minor influence on P_{CO2} thresholds (Fig. 2*B*; *SI Text*, *Sensitivity Tests*).

At 10 °C and a salinity of 10 g/kg, an accumulation rate of 1 cm/y and sedimentary porosity of 60% the upper limit on P_{CO2} levels where siderite production remains below XRD detection limits in the Sheepbed member is 70 mbar. This falls to 10 mbar at average sedimentation rates of ∼0.1 cm/y. Our P_{CO2} estimates are orders of magnitude above those based on thermodynamic stability of magnetite with respect to siderite (Fig. 1), but remain well below the 1000s mbar CO_2 levels required by the most optimistic climate simulations to keep the average temperature of early Mars above 273 K for long periods (33); for example, Ramirez et al. (34) model clement conditions at 1.3 bars CO_2, with 20% H_2 as an additional greenhouse gas.

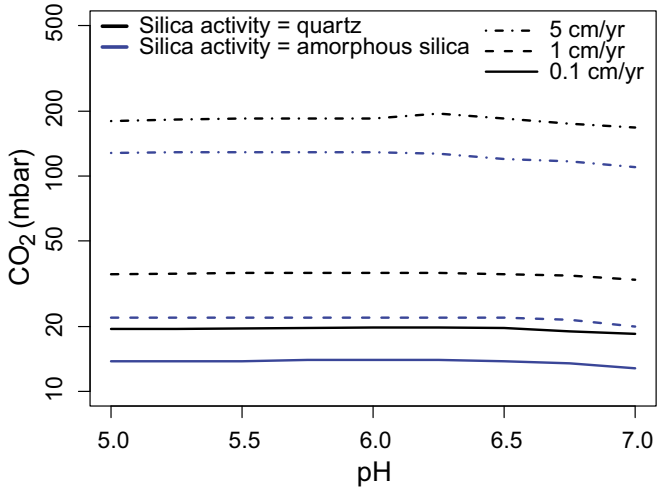

Fig. 3. P_{CO2} required to produce 1 wt % siderite within model sedimentary profiles at various sediment accumulation rates, sediment porosities, and water column pH values. $[Fe^{2+}]$ is set at equilibrium with fayalite with silica saturation in equilibrium with quartz (black lines) and amorphous silica (blue lines). Sedimentary porosity is set at 0.6 in all simulations.

As discussed above, our models and choice of input parameters are designed to provide an absolute upper limit P_{CO2} based on observed mineralogy and sedimentology at YKB. However, there are various reasons to believe that $[Fe^{2+}]$ was higher in pore waters and P_{CO2} may have been lower than the thresholds shown in Fig. 2. First, it is possible that magnetite and hematite detected in YKB sediments (9) are detrital phases that do not place bounds on pore water $[Fe^{2+}]$ or act as a sink for Fe. This would allow for more reducing conditions, higher $[Fe^{2+}]$ (Fig. S2) and lower P_{CO2} thresholds. Second, if the supply of $[Fe^{2+}]$ from olivine outstripped removal by secondary phases (i.e., olivine dissolution kinetics >> precipitation of secondary phases), $[Fe^{2+}]$ would also be higher than in our upper threshold P_{CO2} simulations. In both these cases $[Fe^{2+}]$ would tend toward approaching levels of olivine saturation, thus providing a reduced P_{CO2} threshold limit for a given sedimentation rate, porosity, salinity, and temperatures. Model $[Fe^{2+}]$ for this lower P_{CO2} threshold based on olivine saturation requires an assumption about $[SiO_{2(aq)}]$ of pore waters to be made, but in natural near-surface pore waters $[SiO_{2(aq)}]$ is typically between saturation with respect to quartz or amorphous silica. Both these situations can be used to obtain a pH-dependent expression to determine $[Fe^{2+}]$:

$$\text{Fayalite} + 4[H^+] = 2[Fe^{2+}] + \text{Quartz} + 2[H_2O], \quad [5]$$

or

$$\text{Fayalite} + 4\,[H^+] = 2[Fe^{2+}] + \text{Amorphous silica} + 2[H_2O], \quad [6]$$

$$[Fe^{2+}] = \sqrt{K_{reaction}}\,.[H^+]^4, \quad [7]$$

where $K_{reaction}$ is the reaction constant of either Eq. **5** or **6**. The resulting P_{CO2} thresholds are shown in Fig. 3. With comparable porosity and burial rates P_{CO2} thresholds are approximately half the values calculated assuming pore water $[Fe^{2+}]$ at magnetite saturation. This reinforces our estimates that the martian atmosphere contained 10s mbar levels at the time of deposition of YKB sediments.

Fluvial–lacustrine sediments in Gale Crater represent one of the youngest known instances of habitable surficial aqueous conditions on Mars, on the tail end of a period of rapid atmospheric degradation and loss (6, 12, 33). Thus, our P_{CO2} estimate serves as a reference point at a critical juncture in martian atmospheric evolution. Combining ∼10s mbar estimates of P_{CO2} derived from Gale Crater with upper estimates of the amount of CO_2 lost through sequestration as carbonate minerals in the martian crust (up to ∼500 mbar CO_2; ref. 35) and CO_2 lost to space (<100 mbar; ref. 36) limits atmospheric CO_2 during the Noachian and Early Hesperian to 100s mbar. This is well below threshold levels required to keep the average temperature of early Mars above 273 K for long periods in climate models, therefore either lacustrine features of Gale formed in a cold environment (37) or the problem of reconciling Mars' early climate with geological record of an active hydrosphere remains. Our results imply that the overall lack of carbonates found in the geological record of Mars (5, 6, 28, 35) is a direct reflection of the composition of the ancient atmosphere.

ACKNOWLEDGMENTS. We acknowledge the support of the Jet Propulsion Lab engineering and MSL operations staff. Thanks to K. Zahnle, E. Kite, and M. Daswani for discussions, and constructive reviews from I. Halevy, J. Kasting, P. Niles, and two anonymous reviewers on this and a previous version of the manuscript. We thank P. Sadler for advice and access to sedimentation rate data. Modeling efforts were supported by a NASA Habitable Worlds grant (T.F.B.). This work was supported by the Project "icyMARS" European Research Council Starting Grant 307496 (to A.G.F.). This research was

supported by the NASA Mars Exploration Program. Some of this research was carried out at the Jet Propulsion Laboratory, California Institute of Technology, under a contract with the National Aeronautics and Space Administration.

1. Carr MF (1996) *Water on Mars* (Oxford Univ Press, New York).
2. Di Achille G, Hynek BM (2010) Ancient ocean on Mars supported by global distribution of deltas and valleys. *Nat Geosci* 3:459–463.
3. Bibring J-P, et al. (2006) Global mineralogical and aqueous mars history derived from OMEGA/Mars Express data. *Science* 312(5772):400–404.
4. Murchie SL, et al. (2009) A synthesis of Martian aqueous mineralogy after 1 Mars year of observations from the Mars Reconnaissance Orbiter. *J Geophys Res* 114(E2): 10.1029/2009JE003342.
5. Niles PB, et al. (2012) Geochemistry of carbonates on Mars: Implications for climate history and nature of aqueous environments. *Space Sci Rev* 174(1):301–328.
6. Hu R, Kass DM, Ehlmann BL, Yung YL (2015) Tracing the fate of carbon and the atmospheric evolution of Mars. *Nat Commun* 6(10003):10003.
7. Ehlmann BL, et al. (2011) Subsurface water and clay mineral formation during the early history of Mars. *Nature* 479(7371):53–60.
8. Grotzinger JP, et al. (2015) Deposition, exhumation, and paleoclimate of an ancient lake deposit, Gale crater, Mars. *Science* 350(6257):aac7575.
9. Vaniman DT, et al.; MSL Science Team (2014) Mineralogy of a mudstone at Yellowknife Bay, Gale crater, Mars. *Science* 343(6169):1243480.
10. Treiman AH, et al. (2016) Mineralogy, provenance, and diagenesis of a potassic basaltic sandstone on Mars: CheMin X-ray diffraction of the Windjana sample (Kimberley area, Gale Crater). *J Geophys Res Planets* 121(1):75–106.
11. McLennan SM, et al.; MSL Science Team (2014) Elemental geochemistry of sedimentary rocks at Yellowknife Bay, Gale crater, Mars. *Science* 343(6169):1244734.
12. Grotzinger JP, et al.; MSL Science Team (2014) A habitable fluvio-lacustrine environment at Yellowknife Bay, Gale crater, Mars. *Science* 343(6169):1242777.
13. Bristow TF, et al. (2015) The origin and implications of clay minerals from Yellowknife Bay, Gale crater, Mars. *Am Mineral* 100(4):824–836.
14. Treiman AH, et al. (2014) Ferrian saponite from the Santa Monica Mountains (California, U.S.A., Earth): Characterization as an analog for clay minerals on Mars with application to Yellowknife Bay in Gale Crater. *Am Mineral* 99(11-12):2234–2250.
15. Delany JM, Lundeen SR (1989) The LLNL Thermochemical Database. Lawrence Livermore National Laboratory Report UCRL-21658.
16. Wilson J, Savage D, Cuadros J, Shibata M, Ragnarsdottir KV (2006) The effect of iron on montmorillonite stability. (I) Background and thermodynamic considerations. *Geochim Cosmochim Acta* 70(2):306–322.
17. Rye R, Kuo PH, Holland HD (1995) Atmospheric carbon dioxide concentrations before 2.2 billion years ago. *Nature* 378(6557):603–605.
18. Ohmoto H, Watanabe Y, Kumazawa K (2004) Evidence from massive siderite beds for a CO2-rich atmosphere before approximately 1.8 billion years ago. *Nature* 429(6990): 395–399.
19. Rosing MT, Bird DK, Sleep NH, Bjerrum CJ (2010) No climate paradox under the faint early Sun. *Nature* 464(7289):744–747.
20. Sheldon ND (2006) Precambrian paleosols and atmospheric CO_2 levels. *Precam Res* 147(1-2):148–155.
21. Kasting JF (2010) Early earth: Faint young sun redux. *Nature* 464(7289):687–689.
22. Reinhard CT, Planavsky NJ (2011) Mineralogical constraints on Precambrian pCO_2. *Nature* 474(7349):E1–E2, discussion E4–E5.
23. Borlina CS, Ehlmann BL, Kite ES (2015) Modeling the thermal and physical evolution of Mount Sharp's sedimentary rocks, Gale crater, Mars: Implications for diagenetic minerals on the MSL Curiosity Rover traverse. *J Geophys Res* 120(8):1396–1414.
24. Freissinet C, et al. (2015) Organic molecules in the Sheepbed Mudstone, Gale Crater, Mars. *J Geophys Res Planets* 120(3):495–514.
25. Gautier Q, Bénézeth P, Mavromatis V, Schott J (2014) Hydromagnesite solubility product and growth kinetics in aqueous solution from 25 to 75°C. *Geochim Cosmochim Acta* 138:1–20.
26. Jimenez-Lopez C, Romanek ChS (2004) Precipitation kinetics and carbon isotope partitioning of inorganic siderite at 25°C and 1 atm. *Geochim Cosmochim Acta* 68: 557–571.
27. Ming DW, et al.; MSL Science Team (2014) Volatile and organic compositions of sedimentary rocks in Yellowknife Bay, Gale crater, Mars. *Science* 343(6169):1245267.
28. Fairén AG, Fernández-Remolar D, Dohm JM, Baker VR, Amils R (2004) Inhibition of carbonate synthesis in acidic oceans on early Mars. *Nature* 431(7007):423–426.
29. Hurowitz JA, Fischer WW, Tosca NJ, Milliken RE (2010) Origin of acidic surface waters and the evolution of atmospheric chemistry on early Mars. *Nat Geosci* 3:323–326.
30. Yang L, Steefel CI (2008) Kaolinite dissolution and precipitation kinetics at 22 degrees C and pH 4. *Geochim Cosmochim Acta* 72:99–116.
31. Potter PE, Maynard JB, Depetris PJ (2005) *Mud and Mudstones, Introduction and Overview* (Springer, New York).
32. Sadler PM (1981) Sediment accumulation rates and the completeness of stratigraphic sections. *J Geol* 89:569–584.
33. Haberle RA, Catling DC, Carr MH, Zahnle K (2017) The early Mars climate system. *The Atmosphere and Climate of Mars*, eds Haberle RA, Clancy RT, Forget F, Smith MD, Zurek RW (Cambridge Univ Press, Cambridge, UK), in press.
34. Ramirez RM, et al. (2014) A CO_2-H_2 greenhouse for early Mars. *Nat Geosci* 7:59–63.
35. Edwards CS, Ehlmann BL (2015) Carbon sequestration on Mars. *Geology* 43:863–866.
36. Lammer H, et al. (2013) Outgassing history and escape of the martian atmosphere and water inventory. *Space Sci Rev* 174:113–154.
37. Fairén AG, et al. (2014) A cold hydrological system in Gale crater, Mars. *Planet Space Sci* 93-94:101–118.
38. R Development Core Team (2011) *R: A Language and Environment for Statistical Computing* (R Foundation for Statistical Computing, Vienna, Austria).
39. Soetaert K, Meysman F (2009) *ReacTran: Reactive transport modelling in 1D, 2D and 3D* (R package version 1.4.2).
40. Soetaert K, Petzoldt T, Meysman F (2010) *marelac: Tools for Aquatic Sciences* (R package version 2.1.5).
41. Gattuso et al (2015) *seacarb: Seawater Carbonate Chemistry* (R package version 3.0.11).
42. Hofmann AF, Meysman FJR, Soetaert K, Middleburg JJ (2008) A step-by-step procedure for pH model construction in aquatic systems. *Biogeosciences* 5:227–251.
43. Zeebe RE, Wolf-Gladrow D (2001) *CO2 in Seawater: Equilibrium, Kinetics, Isotopes*. Elsevier Oceanography Series 65 (Elsevier, Amsterdam).
44. Bénézeth P, Dandurand JL, Harrichoury JC (2009) Solubility product of siderite ($FeCO_3$) as a function of temperature (25–250 °C). *Chem Geol* 265:3–12.
45. Silva CAR, Liu XW, Millero FJ (2002) Solubility of siderite ($FeCO_3$) in NaCl solutions. *J Solution Chem* 31:97–108.
46. Dick JM (2015) CHNOSZ: Chemical Thermodynamics and Activity Diagrams (R package version 1.0.7).
47. Hunter KS, Wang Y, Van Cappellen P (1998) Kinetic modeling of microbially-derived redox chemistry of subsurface environments: Coupling transport, microbial metabolism and geochemistry. *J Hydrol (Amsterdam)* 209:53–80.
48. Liu C, Kota S, Zachara JM, Fredrickson JK, Brinkman CK (2001) Kinetic analysis of the bacterial reduction of goethite. *Environ Sci Technol* 35(12):2482–2490.
49. Matsunaga T, Karametaxas G, von Gunten HR, Lichtner PC (1993) Redox chemistry of iron and manganese minerals in river-recharged aquifers: A model interpretation of a column experiment. *Geochim Cosmochim Acta* 57:1691–1704.
50. Johnson ML (1990) Ferrous Carbonate Precipitation Kinetics. A Temperature Ramped Approach. Ph.D. thesis. (Rice University, Houston, TX).
51. Bandstra JZ, Brantley SL (2008) Data fitting techniques with applications to mineral dissolution kinetics. *Kinetics of Water-Rock Interaction*, eds Brantley SL, Kubicki JD, White AF (Springer, New York).
52. ten Berge HFM, et al. (2012) Olivine weathering in soil, and its effects on growth and nutrient uptake in Ryegrass (Lolium perenne L.): A pot experiment. *PLoS One* 7(8): e42098.
53. Helgson HC (1978) Summary and critique of the thermodynamic properties of rock-forming minerals. *Am J Sci* 278A:1–229.